Broad Multiwavelength Second-Harmonic Generation From Two-Dimensional $\chi^{(2)}$ Nonlinear Photonic Crystals of Tetragonal Lattice Structure

Lung-Han Peng, *Member, IEEE*, Chao-Ching Hsu, and Andrew H. Kung, *Member, IEEE*

***Abstract*—We investigate the effects of lattice spacing and domain-filling ratio on the wavelength dependence in second-harmonic generation (SHG) from two-dimensional $\chi^{(2)}$ nonlinear photonic crystals (2-D NPC) on lithium niobate. Spectral coverage of 150 and 200 nm around 1.5 and 1.9 μm in quasi-phase-matched (QPM) SHG is obtained by angular rotation of the NPC with a lattice periodicity of 20×20 and 29.5×29.5 μm^2, respectively. The SHG signals are shown to have off-axial propagation directions determined by the incident wavelength and the QPM vector. The intensity of the high-order reciprocal-lattice-vector $(\mathbf{G_{mn}})$-assisted SHG signal is shown to depend on the domain-filling ratio. These observations are attributed to the unique dispersion of $\mathbf{G_{mn}}$ together with the nonzero $\chi^{(2)}(\mathbf{G_{mn}})$ nonlinearity in the 2-D QPM-NPC having a tetragonal lattice structure.**

***Index Terms*—Nonlinear photonic crystals, quasi-phase-matching, second-harmonic generation (SHG).**

I. Introduction

THE USE OF THE quasi-phase-matching (QPM) technique to enhance nonlinear wave interactions has been actively pursued in nonlinear optics. A QPM structure can be realized in nonlinear crystals by seeking a periodic domain reversal at every coherent length l_c [1]. For the case of second-harmonic generation (SHG), the coherent length is defined as follows:

$$l_c = \frac{\pi}{(k_{2\omega} - 2k_{1\omega})} = \frac{\lambda_\omega}{4(n_{2\omega} - n_{1\omega})} \tag{1}$$

where the $k_{i\omega}$'s and $n_{i\omega}$'s are the wave vectors and refractive indices at the fundamental and second-harmonic frequencies, respectively, and λ_ω is the wavelength of the fundamental beam. This process has been named periodic poling when the QPM structure is realized by the application of an electric field in a ferroelectric crystal to periodically reverse the domain structures. Such material modification can lead to a periodic sign reversal in the spontaneous polarization (P_s) and, therefore, in the $\chi^{(2)}$ nonlinearity. The artificial distribution of the $\chi^{(2)}$ nonlinearity can give rise to a structural symmetry in $\chi^{(2)}$ that is different from the original crystal. This new symmetry can render a structure-imposed phase factor to compensate the destructive interference caused by the material's optical dispersion as the interacting waves propagate in the crystal. For example, the SHG process can be realized by a momentum conservation of $2\mathbf{k}_{1\omega} + \mathbf{G} = \mathbf{k}_{2\omega}$, where $\mathbf{G} = 2\pi/\Lambda$ is the reciprocal lattice vector of a first-order QPM structure with a periodicity of Λ. One advantage in utilizing the QPM mechanism is that it allows access to the largest diagonal matrix element of the nonlinear coefficient, such as d_{33}, which would not be possible in the conventional birefringent phase matching scheme. The reason is that generally in order to satisfy birefringent phase matching, orthogonal polarizations in the interacting waves are required [2]. The nonlinear wave interaction can, thus, only be initiated via coupling with the off-diagonal matrix elements in the nonlinear coefficient, which usually is smaller than its diagonal parts. Applying the QPM mechanism to nonlinear interactions can, therefore, be an efficient means for laser wavelength conversion. Recent realization of QPM optical parametric oscillators (OPO) [3] and second-harmonic generators [4] using periodically poled lithium niobate (PPLN) and potassium titanyl phosphate (PPKTP) [5] are representative developments in this field. A subtle difficulty that has limited the use of one-dimensional (1-D) QPM devices, however, is the tight temperature stability and wavelength acceptance bandwidth. The tolerance in these two factors is approximately equal to $\Lambda/l\,(\sim 0.1\%)$ where l is the length of the crystal [6]. These tight tolerances add to the complexity in system designs where the temperature stability and capacity for simultaneous multiwavelength switching/conversion are concerns for applications in optical information processing [7], [8] and telecommunication [9], [10].

An approach to overcome the issue of a tight wavelength acceptance bandwidth is to engineer a domain configuration such that momentum conservation can be simultaneously satisfied by a number of different wavelengths [11]. This concept can be implemented in a 1-D quasi-periodically [12] or aperiodically [13] poled structure. For QPM-SHG in the quasi-periodically poled structure, the momentum conservation mechanism is written as $2\mathbf{k}_{1\omega} + \mathbf{G}_{\mathrm{mn}} = \mathbf{k}_{2\omega}$. The vectors $\mathbf{G}_{\mathrm{mn}}$ are indexed by two integers m and n, and are expressed as follows:

$$G_{\mathrm{mn}} = 2\pi D^{-1}(m + n\tau) \tag{2}$$

where $D = \tau l_A + l_B$ is the "average structure parameter" taken as the sum of the length $l_{A(B)}$ from each of the building blocks (A, B) in the poled crystal and multiplied by an arbitrary irrational number τ [11]. By doing so, multiwavelength

Manuscript received December 19, 2003; revised July 22, 2004. This research was supported by the National Science Council under Grants 92-2215-E-002-013 and M-001-005.

L.-H. Peng and C.-C. Hsu are with the Department of Electrical Engineering and Institute of Electro-Optical Engineering, National Taiwan University, Taipei 106, Taiwan, R.O.C.

A. H. Kung is with the Institute of Atomic and Molecular Sciences, Academia Sinica, Taipei, Taiwan 106, R.O.C. and also with the National Chiao-Tung University, Hsinchu 300, Taiwan, R.O.C.

Digital Object Identifier 10.1109/JSTQE.2004.836001

QPM-SHG [14] and sum frequency generation [15] have been realized in potassium titanyl phosphate (KTP) and lithium tantalate ($LiTaO_3$). However, the temperature stability of such 1-D QPM devices has not yet been investigated. Alternatively, the concept of a plural number of QPM vectors can be realized in a two-dimensional (2-D) periodically poled structure. For a 2-D poled crystal having an *orthorhombic* lattice structure, the corresponding reciprocal lattice vectors $\mathbf{G}_{\mathrm{mn}}$ are

$$\mathbf{G}_{\mathrm{mn}} = 2\pi(\hat{x}a^{-1}m + \hat{y}b^{-1}n) \tag{3}$$

where a and b are the domain periodicity and, hence, the lattice vector in the x- and y-axis direction, respectively, and m and n are two integers. The active QPM components in this case are those reciprocal lattice vectors $\mathbf{G}_{\mathrm{mn}}$ for which the Fourier transformation of the second-order nonlinearity $\chi^{(2)}(\mathbf{G}_{\mathrm{mn}})$ have nonzero values. These 2-D poled structures are called $\chi^{(2)}$ nonlinear photonic crystals (NPC) [16]. It has been noted in [16] that the indexing of $\mathbf{G}_{\mathrm{mn}}$ in the 1-D quasi-periodic lattice is simply the projection of a 2-D periodic crystal on a 1-D axis with an *irrational* slope. The added dimension creates a number of new phenomena in nonlinear wave interaction. For example, the transversely patterned QPM gratings enable a layout of nonlinear physical optics [17]. A 2-D $\chi^{(2)}$ SHG-NPC can support 1-D and 2-D solitons [18]. Wave interactions in a 2-D NPC can result in SH waves that grow and propagate in directions departing from the fundamental beam [19]. Theory further suggests an optimal design of the 2-D poled patterns that can render QPM vectors $\mathbf{G}_{\mathrm{mn}}$ suitable for third- or fourth-harmonic generation [20].

We have recently demonstrated a two-step poling method that can be used for the fabrication of large area NPC. This method consists of first a high-temperature treatment at 1050 °C to introduce a surface inversion layer, followed by a pulse-field poling [21]. The origin of surface domain inversion in this case is due to the thermally induced out-diffusion process [22]. The polarization-induced charge (i.e., $-\nabla \cdot P_s = \rho$) at the domain boundary serves as a potential barrier to restrict the nucleation and motion of an inverted domain at a designated lattice site [23]. One thereby can overcome the issue of domain merging due to the fringe-field effect as is often encountered in the periodic poling process. Inverted domains of various geometric shapes and lattice structures can, thus, be realized. An important consequence of such a domain manipulation capability is to allow the engineering of QPM-NPCs with a designated lattice structure to enhance the temperature tolerance and the acceptance bandwidth. We have thereby demonstrated a wide temperature bandwidth over 150 °C in the SHG of 532 nm from a 2-D $\chi^{(2)}$ NPC of orthorhombic lattice structure on a 500-μm-thick $LiNbO_3$ substrate [24]. A SHG spectral coverage of over $\sim$ 150 nm has recently been observed by angle tuning of a 2-D $\chi^{(2)}$ NPC having a tetragonal lattice structure of 20×20 μm^2 on $LiNbO_3$ [25].

In this paper, we investigate the wavelength tunability of 2-D $\chi^{(2)}$ NPC that are fabricated to quasi-phase-match to generate the second harmonic of laser beams tunable around the 1.5- and 1.9-μm bands at room temperature (30 °C). The experimental details and results will be summarized in Sections II and III, respectively, and followed by a discussion of the lattice spacing effect on the SHG spectral coverage and the dependence of the SHG efficiency on the $\mathbf{G}_{\mathrm{mn}}$ vectors involved in the QPM process in Section IV. We demonstrate that a wide SHG spectral tuning range of over 200 nm can be obtained on NPC samples of a tetragonal lattice structure with a periodicity of 29.5×29.5 μm^2. These results are ascribed to a unique high-order reciprocal lattice vector ($\mathbf{G}_{\mathrm{mn}}$)-assisted QPM-SHG process and the corresponding nonzero second-order nonlinearities of $\chi^{(2)}(\mathbf{G}_{\mathrm{mn}})$ in the 2-D $\chi^{(2)}$ NPC.

II. Experimental

Two sets of 2-D $\chi^{(2)}$ NPCs were fabricated on Z-cut, double-side-polished, congruent-grown undoped $LiNbO_3$ substrates purchased from Crystal Technology (Palo Alto, CA). They were designed to have a tetragonal lattice structure and a first-order periodicity of 20×20 and 29.5×29.5 μm^2, respectively, to quasi-phase-match to generate the second harmonic of 1.5- and 1.9-μm-band beams at room temperature. A typical procedure of the aforementioned two-step poling method is as follows. A thin ($\sim$ 50 nm), 2-D aluminum (Al) electrode was first evaporated onto the $+Z$ face of $LiNbO_3$ by the standard lithography and lift-off process. We then placed the Al-patterned sample inside a quartz tube furnace and let it undergone a heat treatment at 1050 °C for 5 h in an air ambience. This process resulted in a shallow surface inversion layer in the region not covered by the electrode. Although the Al electrode was oxidized and transformed into an Al_2O_3 pattern, it preserved the underlying $LiNbO_3$ in its original polarization state. The microcracks found in the Al_2O_3 electrode then served as a current path for the subsequent pulsed-field poling. The sample was then transferred to a poling apparatus consisting of a pulsed voltage amplifier (Trek, NJ, USA, model 20/20 A for 20-kV and 20-mA output). The poling setup was similar to that originally designed by Myers *et al.* [26], where a lithium chloride liquid electrode was used to make contact with the sample surfaces via a pair of viton o-rings. To stabilize the domain reversal process, a fast turn-on rectifying diode was put in series with the poling apparatus such that relaxation of the inverted domain was inhibited at the moment the poling field was terminated [27].

The SHG measurements were conducted by using a pulsed grating-tuned periodically poled $LiNbO_3$ optical parametric oscillator [28] as the fundamental frequency pump source. The pulse repetition rate was 4 kHz and the pulsewidth was 30 ns. By choosing an appropriate periodicity and adjusting the temperature of the PPLN crystal in the OPO, wavelength spans from 1450 to 1640 nm, and from 1800 to 2000 nm, respectively, could be obtained as the pump wavelengths. The peak power in the 1.5-μm region was 2 kW while that for the 1.9-μm region was 1.2 kW. The poled samples have a length L_{eff} of 6 mm for the 20×20 μm^2 period NPC which was designed for QPM in the 1.5-μm-band pump and a length L_{eff} of 18 mm for the 29.5×29.5 μm^2 period sample for the 1.9-μm-band pump. Both samples had the edges cut and polished parallel to the crystalline x and y axes. The fundamental beam was loosely focused into the polished 2-D NPC sample with a beam waist

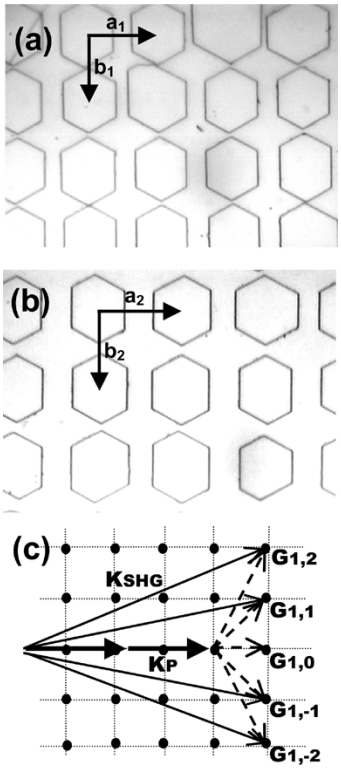

Fig. 1. $-Z$ magnified micrograph showing an NPC consisting of 2-D distribution of inverted domains residing on a tetragonal lattice structure. The lattice vectors a_i and b_i are of equal length and have a center-to-center periodicity of: (a) 20×20 and (b) 29.5×29.5 μm^2 on 300 μm-thick $LiNbO_3$ substrate. (c) QPM-SHG processes in the reciprocal space of NPC showing wave propagation and generation in the NPC.

of ~ 100 μm by a lens of 30-cm focus length, which resulted in a peak intensity of 13.3 MW/cm^2 for the 1.5-μm case and 8 MW/cm^2 for the 1.9-μm case inside the crystal. A rotational stage was attached to the sample mount to vary the azimuth angle of the sample by up to $\pm 15^\circ$, a process equivalent to varying the incident angle of the fundamental beam. The SHG power and the spatial pattern in the far field were recorded at a number of different incident fundamental wavelengths.

III. Results

Illustrated in Fig. 1(a) and (b) are the $-Z$ face micrograph of an NPC showing a distribution of the $\chi^{(2)}$ nonlinearity with a 2-D periodicity of 20×20 and 29.5×29.5 μm^2, respectively. The periodicity is measured as the center-to-center distance of the adjacent inverted domains shown in the figure. A close examination of Fig. 1 indicates the inverted domains are registered on a square (i.e., tetragonal) lattice site. In particular, one notes there is a pinnacle shape of structure residing on the inverted domain, indicating a slightly faster domain growth along the crystal's y axis than the x axis [29]. The ratio of the area of the inverted domain to that spanned by the lattice vectors of the 2-D NPC can be characterized by a factor called the domain-filling ratio. It has been noted in [16] that this filling ratio relates directly to the second-order nonlinearity of $\chi^{(2)}(\mathbf{G}_{\rm mn})$ for a given reciprocal lattice vector $\mathbf{G}_{\rm mn}$ where the QPM-nonlinear process

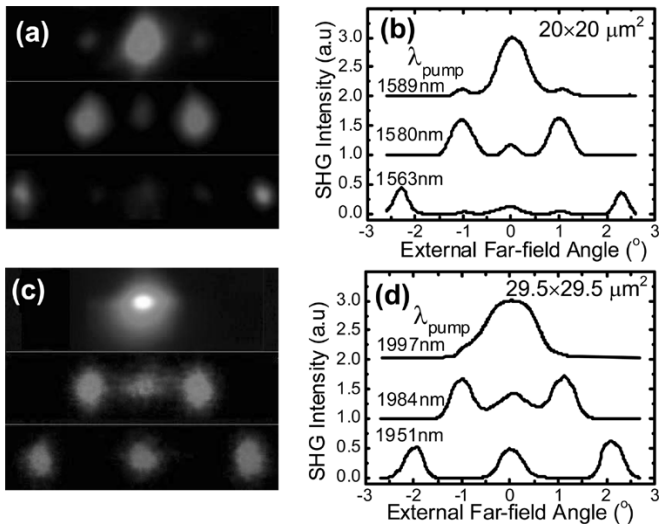

Fig. 2. (a) and (c) CCD images and (b) and (d) normalized far-field SHG intensity distribution for the NPC samples shown in Fig. 1. Details of the experimental conditions and data are shown in Table I.

takes place. This issue will be further alluded to in Section IV of this paper.

Moreover, the spatial distribution of $\chi^{(2)}$ nonlinearity shown in Fig. 1 has a C_{4v} tetragonal symmetry that differs from the C_{3v} trigonal lattice symmetry of the $LiNbO_3$ host crystal. The nonlinear generation and propagation of the interacting waves in this photonic crystal would depend solely on the C_{4v} domain symmetry and is independent of the host's crystal symmetry. Sketched in Fig. 1(c) are the SHG signals and the momentum vectors in the reciprocal space of the NPC showing the high-order $\mathbf{G}_{\rm mn}$-assisted QPM processes. They illustrate simultaneous phase matching and spatial separation of the fundamental and harmonic waves that are unique to the 2-D NPC structure.

Shown in Fig. 2 are the CCD images taken with a digital camera and the normalized far-field intensity distribution of QPM-SHG signals for the $\chi^{(2)}$ NPC samples shown in Fig. 1. The SHG data were measured with the fundamental beam propagating along the crystal's x axis (i.e., 0° incident angle). The images were taken by placing an IR-sensitive florescence card 10 cm away from the sample. Data in Table I summarize the far-field angle $(\theta_\perp)$ and the average SHG power of the 20×20 [Fig. 1(a)] and 29.5×29.5 μm^2 [Fig. 1(b)] period NPC samples with respect to the phase-matched fundamental wavelengths/incident powers and the contributing $\mathbf{G}_{\rm mn}$ vector in the QPM-SHG process. Even though the input intensity of the 1.5- and 1.9-μm-band OPO differed by a factor of two, one can still maintain a SHG output power ~ 50 mW for the $\mathbf{G}_{10}$-assisted QPM process by resorting to a longer interaction length $(L_{\rm eff} \sim 18$ mm$)$ in the latter case.

Referring to Fig. 2(a) and (c), one observes a symmetrical distribution of the 1.5- and 1.9-μm-pump QPM-SHG patterns in a plane *transverse* to the propagation direction of the fundamental beam. By rotating the crystal 90° to let the pump beam propagat along the crystal's y axis, similar transverse distributions of SHG signal were also observed (not shown). This fourfold rotational symmetry reveals the tetragonal structural effect of the 2-D NPC on the SHG process [30]. From the peak

TABLE I
PARAMETERS AND DATA OF QPM-SHG OUTPUT FROM THE 2-D NPCS SHOWN IN FIG. 1

Periodicity	[μm^2]	20×20	29.5×29.5
Effective Length	[mm]	6	18
Incident Intensity	[MW/cm^2]	13.3	7.9
Ave. Pump Power	[mW]	160	120
Beam Waist	[μm]	80	90
QPM Wavelength	[nm]	(1589, 1580, 1563)	(1997, 1984, 1951)
SHG power	[mW]	(66, 16.8, 6.4)	(50, 3.4, 2.0)
Far Field Angle	[°]	(0, ±1.13, ±2.25)	(0, ±0.97, ±1.91)
QPM vectors G_{mn}		(G_{10}, $G_{1,\pm1}$, $G_{1,\pm2}$)	(G_{10}, $G_{1,\pm1}$, $G_{1,\pm2}$)

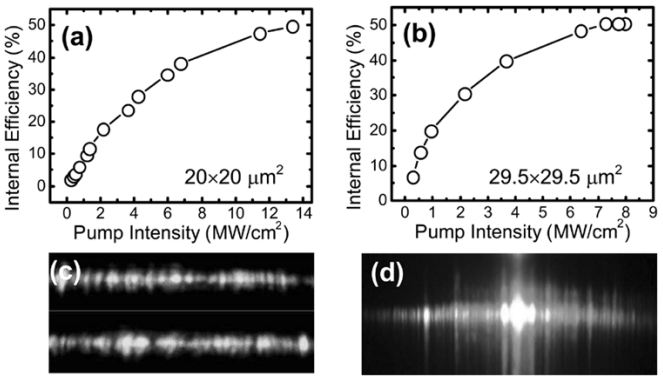

Fig. 3. (a)–(b) Measured internal conversion efficiency for the $\mathbf{G}_{10}$-assisted QPM-SHG process. (c)–(d) *Cascaded-QPM third and fourth* harmonic signals for samples in Fig. 1.

position of the SHG signals shown in Fig. 2(b) and (d), one notes that the associated far-field angles ($\theta_\perp$) and peak SHG intensities exhibit a unique dependence on the QPM wavelengths. That is, $\theta_\perp$ decreases but the peak SHG intensity increases as one sequentially increases the QPM wavelength. Data from Table I show that at an input intensity of 13.3 MW/cm^2, the total power summed from two SHG beams caused by the 1563-nm pump at $\theta_\perp = \pm 2.25°$ is 12.4 mW, whereas the single spot of SHG from the 1590-nm pump has a power of 66 mW at $\theta_\perp = 0°$. Table I only lists the $\theta_\perp$ angles associated with QPM vectors that resulted in the strongest SHG intensity. Other signals had an intensity at least one order of magnitude lower and, hence, were omitted. These latter signals represent a beam deflection of the SH wave by the QPM vector $2\mathbf{k}_{1\omega} + \mathbf{G}_{1,\pm n}$ in the NPC, whereas the intensity distribution carries the information of $\chi^{(2)}(\mathbf{G}_{1,\pm n})$ on the SH conversion. The appearance of mirror symmetry in phase-matching angle and the reduction in conversion efficiency signify a phase-matched SHG mechanism due to contribution from the high-order reciprocal lattice vector $\mathbf{G}_{1,\pm n}$, and the nonzero value of the corresponding $\chi^{(2)}(\mathbf{G}_{1,\pm n})$ nonlinearities. These quantities exhibit the subtle dependence of the QPM-SHG process on the fundamental wavelength and the lattice spacing/symmetry of the NPC.

Further shown in Fig. 3 are the internal efficiency curves for the $\mathbf{G}_{1,0}$-assisted QPM-SHG in the 20×20 [Fig. 1(a)] and 29.5×29.5 μm^2 [Fig. 1(b)] period 2-D NPC sample pumped at a fundamental beam of 1589- and 1998-nm wavelength. Note the conversion efficiency is linear up to a pump intensity of ~ 4 (and 2) MW/cm^2 for the NPC sample in Fig. 3(a) and (b), respectively, and the process approaches saturation with an internal conversion efficiency reaching 50% as the pump intensity increases above 12 (and 8) MW/cm^2. Similar saturation behavior has also been reported on 2-D NPC with *hexagonal* lattice structure. This effect has been ascribed to the increase of parametric back conversion with the SHG power in [19]. Note that in the latter, the maximum internal conversion efficiency reached 41%–82% and saturated at a pump intensity of ~ 1 GW/cm^2 with the 1531-nm picosecond laser.

In addition to the QPM-SHG process, cascaded generation of third and fourth harmonics were also observed. Illustrated in Fig. 3(c) and (d) are the images of mixed third- and fourth-harmonic outputs of green and blue and red and blue light generated by the 1589- and 1997-nm fundamental beams in the 20×20 and 29.5×29.5 μm^2 period 2-D NPC samples, respectively. Note third-harmonic green beams like the ones in Fig. 3(c) showing an almost continuous range of emission angles have also been reported in [19]. Although our NPC devices were originally designed for phase matching to the multiwavelength QPM-SHG process, the abundance of higher order (third and fourth) harmonic generations suggest a potential use for studying the cascaded $\chi^{(2)}$ QPM nonlinear phenomena [31].

To further investigate the wavelength tunability of QPM-SHG in tetragonal $\chi^{(2)}$ NPC, we azimuthally rotated the sample such that the internal incident angle of the input beam relative to the x (or y) axis of the 2-D NPC can be varied. In doing so, each of the allowable QPM-SHG processes can be accessed by a suitable reciprocal lattice vector that fulfills the phase-matching condition of $2\mathbf{k}_{1\omega} + \mathbf{G}_{\rm mn} = \mathbf{k}_{2\omega}$. The above procedure helps to analyze the lattice spacing effect on the wavelength span of QPM-SHG in a 2-D NPC. Illustrated in Fig. 4(a) and (c) are the normalized SHG spectra labeled with the contributing QPM vectors of $\mathbf{G}_{\rm mn}$ for the 20×20 and 29.5×29.5 μm^2 period 2-D NPC samples, showing the angular dependence on the spectral coverage of QPM wavelength. The data were recorded at an azimuthal rotation angle $\phi = 0°$, $-5°$, and $-8°$, respectively. Although we did not measure the full range of SHG wavelengths accessible with the 2-D NPCs, one can clearly discern an increase in the spacing between the QPM wavelengths with the azimuthal rotation angle ϕ. In addition, the measured wavelength span of the QPM-SHG process is shown to increase with the lattice spacing of the 2-D NPC, changing from 150 to 200 nm as the 2-D lattice spacing increases from 20 to 29.5 μm. Here we note the peak intensity of the SHG signals decreases with ϕ for the same $\mathbf{G}_{\rm mn}$ not shown. This is possibly due to an increase in the walk-off angle between the fundamental and the SH waves.

IV. DISCUSSION

In order to quantify the above observations, we applied a ray-tracing method in geometric optics to reveal the underlying physics corresponding to the spatial distribution of the QPM-SHG process [32]. In the calculation, the material's refractive index $n_e(\omega)$ of $LiNbO_3$ was taken from [33]. The reciprocal lattice vectors $\mathbf{G}_{\rm mn}$ was calculated according to (3) by letting the lattice constant (a, b) equal to 20 (or 29.5) μm for the tetragonal $\chi^{(2)}$ NPC used in this work. After taking

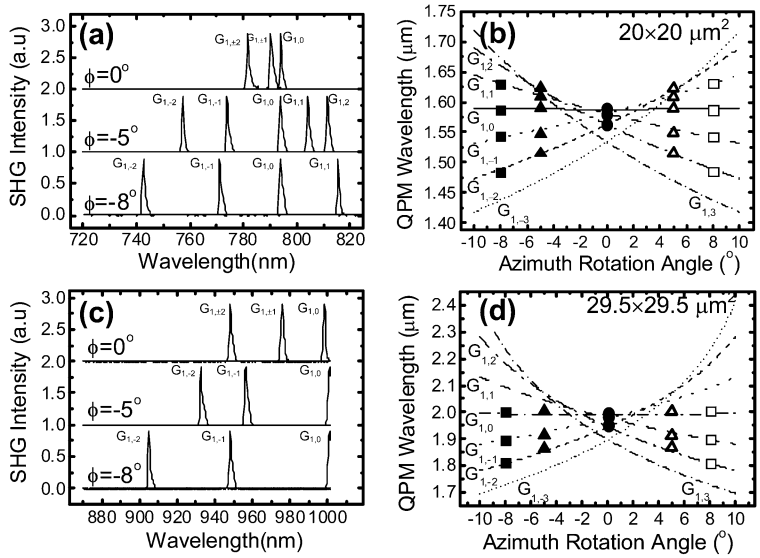

Fig. 4. (a) and (c) Normalized QPM-SHG spectra labeled with the $\mathbf{G}_{\mathrm{mn}}$ vectors. The spectrometer had a detection limit at 1-μm wavelength. (b) and (d) Dispersion curves of $\mathbf{G}_{\mathrm{mn}}$ for NPC samples in Fig. 1. Lines and dots: calculated results; symbols: experimental data.

into account the Fresnel diffraction and the QPM condition of $2\mathbf{k}_{1\omega} + \mathbf{G}_{\mathrm{mn}} = \mathbf{k}_{2\omega}$, one can derive a dispersion curve to reveal the dependence of phase-matching wavelength on the reciprocal lattice vector $\mathbf{G}_{\mathrm{mn}}$ and the azimuthal rotation angle ϕ in the x–y plane. Compared with angular tuning in the conventional birefringent phase-matching scheme, the addition of $\mathbf{G}_{\mathrm{mn}}$ in the NPC signifies the importance of lattice spacing effect on the wavelength coverage of the QPM-SHG process.

A. Lattice Spacing Effect

We illustrate in Fig. 4(b) and (d) the dispersion curves of $\mathbf{G}_{1,0}$, $\mathbf{G}_{1,\pm1}$, $\mathbf{G}_{1,\pm2}$, and $\mathbf{G}_{1,\pm3}$ with respect to the QPM wavelength and rotation angle at a 2-D lattice spacing of 20×20 and 29.5×29.5 μm^2, respectively The calculated curves were overlaid with the experimental data to support our analysis. As the periodicity of NPC is increased, one can clearly observe an increase in the spectral span of the phase-matched wavelengths at a given ϕ. This can be credited to the increase of the slope of $\delta\lambda/\delta\phi$ at each dispersion $\mathbf{G}_{1,\pm n}$ curve with the lattice spacing of the 2-D NPC in lithium niobate. This explains why the NPC of a 29.5×29.5 μm^2 periodicity can have a wider spectral span of over 400 nm in the QPM wavelength than that of 200 nm in the 20×20 μm^2 period NPC at $\phi = 8°$. It is worth pointing out that for each of the $\mathbf{G}_{1,\pm n}$ dispersion curve shown in Fig. 4, one can obtain a continuous SHG wavelength tuning by a continuous change of the incidence angle, or equivalently speaking, by a simple azimuth angle (ϕ) rotation. One can also detect an inversion symmetry in the dispersion curves with respect to ϕ and a crossover of the $\mathbf{G}_{1,\pm n}$ curves at $\phi = 0°$. These are specific properties due to the C_{4v} domain symmetry of the tetragonal structure of our 2-D NPC. Similar crossing behavior in the dispersion curves with respect to the phase-matched temperature and lattice spacing has also been observed in an orthorhombic $\chi^{(2)}$ NPC structure [24]. Referring to Fig. 4(b) and (d), one notes that at $\phi = 0°$ the phase-matching wavelengths become degenerate for each pair of the $\mathbf{G}_{1,\pm n}$ curves. This explains why only three wavelengths were observed in the phase-matched spectra of Fig. 4(a) and (c) at $\phi = 0°$ instead of five at $\phi > 0°$. Our calculations also clarify the increase in the quasi-phase-matched wavelength spectral coverage obtained by a simple crystal rotation. These effects would be beneficial to applications in optical information processing where the channel number and spectral bandwidth become important considerations in the system design [7]–[10].

B. QPM-SHG Efficiency

It has been shown in the case of a noncollinearly pumped 1-D QPM device that the use of a larger aperture pumping scheme can ensure an overlap of the pump, signal, and idler waves in the crystal, thus leading to a desirable optical gain in the OPO [34]. This scheme can allow phase matching at multiple noncollinear angles and result in broadband wavelength output. A similar concept can also be applied to the QPM-SHG process in a 2-D $\chi^{(2)}$ NPC when the high-order $\mathbf{G}_{\mathrm{mn}}$ vectors are involved in the nonlinear optical process. As a rule of thumb, the divergence of the incident beam inside the 2-D NPC (θ_{pump}) should be larger than the angle (θ_{QPM}) of the QPM vector $2\mathbf{k}_{1\omega} + \mathbf{G}_{\mathrm{mn}}$. One thereby can maintain a desirable overlap between the fundamental and SH waves to achieve sufficient nonlinear conversion. This can transform into a simple relation of $(w_0/L_{\mathrm{eff}}) \geqq \theta_{\perp}/n_e$ when the far-field angle ($\theta_{\perp}$) of the $\mathbf{G}_{\mathrm{mn}}$-assisted QPM-SHG process is less than a few tens of milliradians, and w_0 and L_{eff} are the beam waist and effective length of the NPC. With a fundamental pump of 100-μm beam waist, one quickly notices the above criterion is satisfied for the QPM vectors of $\mathbf{G}_{1,\pm1}$ and $\mathbf{G}_{1,\pm2}$ in the $L_{\mathrm{eff}} = 6$ mm NPC sample of 20×20 μm^2 period, whereas in the longer sample of $L_{\mathrm{eff}} = 18$ mm, such relation is not satisfied. This partially explains the quick reduction of the SHG power for the $\mathbf{G}_{1,1}$ and $\mathbf{G}_{1,2}$-assisted SHG processes in the longer NPC sample listed in Table I.

Another factor concerning the SHG output power is the QPM nonlinearity $\chi^{(2)}(\mathbf{G}_{\mathrm{mn}})$. Generally the conversion efficiency is proportional to the square of $\chi^{(2)}(\mathbf{G}_{\mathrm{mn}})$. $\chi^{(2)}(\mathbf{G}_{\mathrm{mn}})$ can be evaluated by performing a 2-D Fourier transform according to

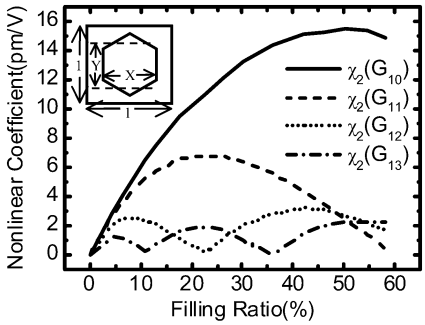

Fig. 5. Calculated second-order nonlinearity $\chi^{(2)}(\mathbf{G}_{\rm mn})$ as a function of the inverted domain-filling ratio whose definition is shown in the inset.

a given NPC domain pattern and the formalism described in [16]. In the analysis, we let the domain-filling ratio, defined as the area ratio of the stretched hexagon to the square unit cell sketched in the inset of Fig. 5, to be a fitting parameter in order to comply with the observation that the inverted domain grows slightly faster along the y axis than in the x axis. Illustrated in Fig. 5 are the calculated $\chi^{(2)}(\mathbf{G}_{\rm mn})$ curves showing the domain-filling ratio effects on the second-order nonlinearity at various $\mathbf{G}_{\rm mn}$ vectors. Note there appears a strong dependence of the $\chi^{(2)}(\mathbf{G}_{1,0})$, $\chi^{(2)}(\mathbf{G}_{1,1})$, $\chi^{(2)}(\mathbf{G}_{1,2})$, and $\chi^{(2)}(\mathbf{G}_{1,3})$ values on the domain-filling ratio. We note the $\chi^{(2)}(\mathbf{G}_{1,1})$ has a fast falling slope while the $\chi^{(2)}(\mathbf{G}_{1,0})$ and $\chi^{(2)}(\mathbf{G}_{1,2})$ curves reach a maximum around a domain-filling ratio of 40%. However, at this filling ratio, the $\chi^{(2)}(\mathbf{G}_{1,3})$ value is nearly zero. These observations would affect the generation of SH signals that seek QPM by the higher-order $\mathbf{G}_{\rm mn}$ vectors. For example, the SHG signals caused by the $\chi^{(2)}(\mathbf{G}_{1,3})$ nonlinearity would be much weaker than those obtained by the other $\chi^{(2)}(\mathbf{G}_{1,n})$ components. By comparing the measured SHG power at various $\mathbf{G}_{\rm mn}$-assisted QPM processes of the 20×20 μm^2 period NPC sample, whose experimental condition fulfilled the criterion of $(w_0/L_{\rm eff}) \geqq \theta_{\perp}/n_e$, one obtain an equivalent domain-filling ratio of 39.2% that agrees with the SHG signals generated in the unsaturated pump regime. For the longer ($L_{\rm eff} = 18$ mm) NPC sample of 29.5×29.5 μm^2 period, we are currently investigating the use of an elliptical-pump scheme with larger aperture size [34] to retrieve the information of $\chi^{(2)}(\mathbf{G}_{\rm mn})$ at larger QPM vectors and their effects on the high-order harmonic processes. The results will be presented in a forthcoming publication.

V. Conclusion

In summary, we have shown that the lattice spacing and domain-filling ratio in the 2-D NPC play an important role in determining the span of QPM wavelengths and the conversion efficiency. Using 2-D NPCs with tetragonal lattice structure symmetry, we have shown that simultaneous multiwavelength SHG with propagation directions departing from that of the fundamental pump beam is possible. We observe a spectral coverage of over 150 and 200 nm at the 1.5- and 1.9-μm pump band by the rotation of NPC that has a 2-D lattice periodicity of 20×20 and 29.5×29.5 μm^2, respectively. These observations are ascribed to the unique dispersion of $\mathbf{G}_{\rm mn}$ and the nonvanishing nonlinearity $\chi^{(2)}(\mathbf{G}_{\rm mn})$ of the 2-D NPC.

References

[1] J. A. Armstrong, N. Bloembergen, J. Ducuing, and P. S. Pershan, "Interactions between light waves in a nonlinear dielectric," *Phys. Rev.*, vol. 127, pp. 1918–1939, 1962.

[2] D. A. Roberts, "Simplified characterization of uniaxial and biaxial nonlinear optical crystals: A plea for standardization of nomenclature and conventions," *IEEE J. Quantum Electron.*, vol. 28, pp. 2057–2074, Oct. 1992.

[3] L. E. Myers and W. R. Bosenberg, "Periodically poled lithium niobate and quasi-phase-matched optical parametric oscillators," *IEEE J. Quantum Electron.*, vol. 33, pp. 1663–1672, Oct. 1997.

[4] M. Yamada, N. Nada, M. Saitoh, and K. Watanabe, "First-order quasiphase matched $LiNbO_3$ waveguide periodically poled by applying an external field for efficient blue second-harmonic generation," *Appl. Phys. Lett.*, vol. 62, pp. 435–436, 1993.

[5] G. Rosenman, A. Skliar, M. Oran, and M. Katz, "Polarization reversal in $KTiOPO_4$ crystals," *J. Phys. D: Appl. Phys.*, vol. 30, pp. 277–82, 1997.

[6] M. M. Fejer, G. A. Magel, D. H. Jundt, and R. L. Byer, "Quasi-phase-matched second harmonic generation: tuning and tolerances," *IEEE J. Quantum Electron.*, vol. 28, pp. 2631–2654, Nov. 1992.

[7] S. M. Saltiel and Y. S. Kivshar, "All-optical deflection and splitting by second-order cascading," *Opt. Lett.*, vol. 27, pp. 921–923, 2002.

[8] A. Chowdhury, C. Staus, B. F. Boland, T. F. Kuech, and L. McCaughan, "Experimental demonstration of 1535–1555 nm simultaneous optical wavelength interchange with a nonlinear photonic crystal," *Opt. Lett.*, vol. 26, pp. 1353–1355, 2001.

[9] M. H. Chou, K. R. Parameswaran, M. M. Fejer, and I. Brener, "Multiple-channel wavelength conversion by use of engineered quasiphase-matching structures in $LiNbO_3$ waveguide," *Opt. Lett.*, vol. 24, pp. 1157–1159, 1999.

[10] B. Chen, C. Q. Xu, B. Zhou, and X. H. Tang, "Analysis of cascaded second-order nonlinear interaction based on quasi-phase-matched optical waveguides," *IEEE J. Select. Topics Quantum Electron.*, vol. 8, pp. 675–680, May/June 2002.

[11] K. Fradkin-Kashi, A. Arie, P. Urenski, and G. Rosenman, "Multiple nonlinear optical interactions with arbitrary wave vector differences," *Phys. Rev. Lett.*, vol. 88, pp. 02 390-1–023 903-4, 2002.

[12] Y.-Q. Qin, Y.-Y. Zhu, S.-N. Zhu, and N.-B. Ming, "Quasiphase-matched harmonic generation through coupled parametric process in a quasiperiodic optical superlattice," *J. Appl. Phys.*, vol. 84, pp. 6911–6916, 1998.

[13] B.-Y. Gu, Y. Zhang, and B.-Z. Dong, "Investigation of harmonic generations in aperiodic optical superlattice," *J. Appl. Phys.*, vol. 87, pp. 7629–7637, 2000.

[14] H. Liu, S. N. Zhu, Y. Y. Zhu, N. B. Ming, X. C. Lin, W. J. Ling, A. Y. Yao, and Z. Y. Xu, "Multiple-wavelength second-harmonic generation in aperiodic optical superlattice," *Appl. Phys. Lett.*, vol. 81, pp. 3326–3328, 2002.

[15] J. Liao, J.-L. He, H. Liu, H.-T. Wang, S. N. Zhu, Y. Y. Zhu, and N. B. Ming, "Simultaneous generation of red, green, and blue quais-continuous-wave coherent radiation based on multiple quasiphase-matched interactions from a single, aperiodically-poled $LiTaO_3$," *Appl. Phys. Lett.*, vol. 82, pp. 3159–3161, 2003.

[16] V. Berger, "Nonlinear photonic crystals," *Phys. Rev. Lett.*, vol. 81, pp. 4136–4139, 1998.

[17] J. R. Kurz, A. M. Schober, D. S. Hum, A. J. Saltzman, and M. M. Fejer, "Nonlinear physical optics with transversely patterned quasi-phase-matching gratings," *IEEE J. Select. Topics Quantum Electron.*, vol. 8, pp. 660–663, May/June 2002.

[18] B. A. Malomed, P. G. Kevrekidis, D. J. Frantzeskakis, H. E. Nistazakis, and A. Y. Yannacopoulos, "One and two-dimensional solitons in second-harmonic-generating attics," *Phys. Rev. E*, vol. 65, pp. 056 606–056 606, 2002.

[19] N. G. R. Broderick, G. W. Ross, H. L. Offerhaus, D. J. Richardson, and D. C. Hanna, "Hexagonally poled lithium niobate: A two-dimensional nonlinear photonic crystal," *Phys. Rev. Lett.*, vol. 84, pp. 4136–4139, 2000.

[20] A. H. Norton and C. M. De Sterke, "Two-dimensional poling patterns for 3rd and 4th harmonic generation," *Opt. Exp.*, vol. 11, pp. 1008–1014, 2003.

[21] L.-H. Peng, Y.-C. Shih, and Y.-C. Zhang, "Restrictive domain motion in polarization switching of lithium niobate," *Appl. Phys. Lett.*, vol. 81, pp. 1666–1668, 2002.

[22] K. Nakamura, H. Ando, and H. Shimizu, "Ferroelectric domain inversion caused in $LiNbO_3$ plates by heat treatment," *Appl. Phys. Lett.*, vol. 50, pp. 1413–1414, 1987.
[23] L.-H. Peng, Y.-C. Shih, S.-M. Tsan, and C.-C. Hsu, "Mitigation of transverse domain growth in two-dimensional polarization switching of lithium niobate," *Appl. Phys. Lett.*, vol. 81, pp. 5210–5212, 2002.
[24] L.-H. Peng, C.-C. Hsu, and Y.-C. Shih, "Second-harmonic green generation from two-dimensional $\chi^{(2)}$ nonlinear photonic crystal with orthorhombic lattice structure," *Appl. Phys. Lett.*, vol. 83, pp. 3447–3449, 2003.
[25] L.-H. Peng, C.-C. Hsu, J. Ng, and A. H. Kung, "Wavelength tunability of second-harmonic generation from two-dimensional $\chi^{(2)}$ nonlinear photonic crystals with a tetragonal lattice structure," *Appl. Phys. Lett.*, vol. 84, pp. 3250–3252, 2004.
[26] L. E. Myers, R. C. Eckardt, M. M. Fejer, R. L. Byer, W. R. Bosenberg, and J. W. Pierce, "Quasiphase-matched optical parametric oscillators in bulk periodically poled $LiNbO_3$," *J. Opt. Soc. Amer. B*, vol. 12, pp. 2102–2116, 1995.
[27] L.-H. Peng, Y.-C. Zhang, and Y.-C. Lin, "Zinc oxide doping effects in polarization switching of lithium niobate," *Appl. Phys. Lett.*, vol. 78, pp. 4–6, 2001.
[28] C.-S. Yu and A. H. Kung, "Grazing-incidence periodically poled $LiNbO_3$ optical parametric oscillator," *J. Opt. Soc. Amer. B*, vol. 16, pp. 2233–2238, 1999.
[29] V. Y. Shur, E. L. Rumyantsev, R. G. Batchko, G. D. Miller, M. M. Fejer, and R. L. Byer, "Domain kinetics in the formation of a periodic domain structure in lithium niobate," *Phys. Solid State*, vol. 41, pp. 1681–1687, 1999.
[30] J. F. Nye, *Physical Properties of Crystals*. Oxford, U.K.: Oxford Univ. Press, 1989.
[31] N. G. R. Broderick, R. T. Bratfalean, T. M. Monro, D. J. Richardson, and C. M. De Sterke, "Temperature and wavelength tuning of second-, third-, and fourth-harmonic generation in a two-dimensional hexgonally poled nonlinear crystal," *J. Opt. Soc. Amer. B.*, vol. 19, pp. 2263–2272, 2002.
[32] E. Hecht, *Optics*. Reading, MA: Addison-Wesley, 1997.
[33] D. H. Jundt, "Temperature-dependent Sellmeier equation for the index of refraction, n_e, in congruent lithium niobate," *Opt. Lett.*, vol. 22, pp. 1553–1555, 1997.
[34] S. M. Russell, P. E. Powers, M. J. Missey, and K. L. Schepler, "Broadband mid-infrared generation with two-dimensional quasi-phase-matched structures," *IEEE J. Quantum Electron.*, vol. 37, pp. 877–887, July 2001.

Lung-Han Peng (S'88–M'95) was born in Taiwan, R.O.C., in 1964. He received the B.S. degree in electrical engineering from National Taiwan University, Taipei, in 1986 and the Ph.D. degree in applied physics from Harvard University, Cambridge, MA, in 1994.

He was a Visiting Scientist at the Massachusetts Institute of Technology, Cambridge, in 1994 and a Postdoctoral Research Fellow at Oak Ridge National Laboratory, Oak Ridge, TN, in 1995. He is currently a Professor with the Graduate Institute of Electro-Optical Engineering and Department of Electrical Engineering, National Taiwan University. His research interests include semiconductor optics and nonlinear optics.

Chao-Ching Hsu was born in Taiwan, R.O.C., in 1979. He received the B.S. and M.S degrees in electrical engineering and electrooptical engineering, respectively, from National Taiwan University, Taipei, in 2001 and 2003, respectively. He is currently working toward the Ph.D. degree at National Taiwan University.

Mr. Hsu's research interests are in the fabrication and characterization of nonlinear photonic crystal.

Andrew H. Kung (M'73) was born in Shanghai, China. He received the Ph.D. degree in electrical engineering from Stanford University, Stanford, CA, in 1973.

He was a Postdoctoral Research Fellow in the Ginzton Laboratory, Stanford University (1973–1975), a Senior Scientist in the Molecular Materials and Chemical Sciences Divisions of Lawrence Berkeley Laboratory, Berkeley, CA (1975–1994), and directed the Laser Center at the Chemistry Department of the University of California, Berkeley (1980–1989). He is now a Research Fellow at the Institute of Atomic and Molecular Sciences of the Academia Sinica, Taipei, Taiwan, R.O.C., and an Adjunct Professor with the National Chiao-Tung University, Hsinchu, Taiwan, R.O.C. His research interests include nonlinear optics, spectroscopy, and laser physics.

Dr. Kung is a Fellow of the American Physical Society and the Optical Society of America.